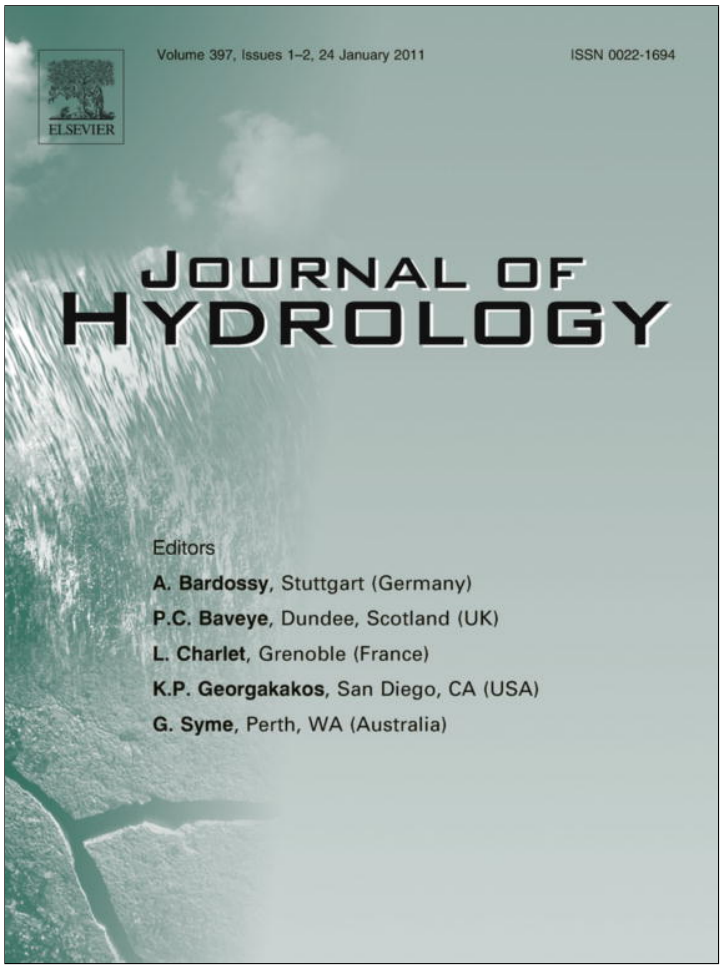

Journal of Hydrology 397 (2011) 10–22

Contents lists available at ScienceDirect

Journal of Hydrology

journal homepage: www.elsevier.com/locate/jhydrol

# Remote sensing estimates of supplementary water consumption by arid ecosystems of central Argentina

Sergio Contreras [a,b,*], Esteban G. Jobbágy [a], Pablo E. Villagra [c], Marcelo D. Nosetto [a], Juan Puigdefábregas [d]

[a] Grupo de Estudios Ambientales, Instituto de Matemática Aplicada de San Luis, Universidad Nacional de San Luis & CONICET, San Luis, Argentina
[b] Bureau of Economic Geology, Jackson School of Geosciences, University of Texas at Austin, Austin, USA
[c] Departamento de Dendrocronología e Historia Ambiental, Centro Regional de Investigaciones Científicas y Tecnológicas, CONICET, Mendoza, Argentina
[d] Departamento de Desertificación y Geoecología, Estación Experimental de Zonas Áridas, Consejo Superior de Investigaciones Científicas, Almería, Spain

ARTICLE INFO

*Article history:*
Received 12 April 2010
Received in revised form 16 August 2010
Accepted 20 November 2010

This manuscript was handled by K. Georgakakos, Editor-in-Chief, with the assistance of Christa D. Peters-Lidard, Associate Editor

*Keywords:*
Evapotranspiration
Inflow dependent ecosystems
Remote sensing
MODIS
Enhanced Vegetation Index
Hydrological equilibrium hypothesis

SUMMARY

Besides precipitation inputs, evapotranspiration of irrigated and natural oases, i.e. riparian and phreatophytic ecosystems, of rain-shadow deserts is strongly influenced by lateral water inputs supplied by mountain rivers and foothill-recharged aquifers. A better understanding of these supplies and their imprint on the water consumption of those inflow dependent ecosystems (IDEs) across arid regions is critical to manage agricultural outputs and ecosystem conservation, and the hydrological trade-offs that emerge among them. Actual operative satellite and physically-based algorithms able to map evapotranspiration (ET) rates at regional scales still fail when they are applied in ungauged regions because of their high parameterization and meteorological data requirements. We introduce an ecological and satellite-based approach to explore the impacts of external water supplies on arid ecosystems, focusing on the Central Monte desert and its water supplies from the Andean Cordillera, in Argentina. Mean annual precipitation (MAP) and the Enhanced Vegetation Index (EVI) from MODIS imagery, used as a surrogate of ET, were the input variables of our empirical model. Two related biophysical indexes were generated for the whole territory of interest based on a MAP–EVI regional function calibrated for the region: the EVI Anomaly (i.e. deviation from a reference with similar MAP) and the ET Anomaly (i.e. additional water consumption besides MAP). These indexes allowed us to identify IDEs and to quantify the impact of remote lateral inflows as well as local constrains on the water balance of rangelands, and irrigated and natural oases. The performance of this satellite-based approach was evaluated through comparisons with independent ET estimates based on plot (known crop coefficients) and basin (measured water budgets) scale approaches. Relative errors in the 2–18% range at plot and basin scale are in agreement with those uncertainties reported by other satellite and physically-based approaches. Our approach provides a simple yet robust diagnostic tool to characterize water balance in arid regions, aimed to improve the identification of inflow dependent ecosystems and their management under the demanding pressures of land use and climate change.



## 1. Introduction

Meager rainfall inputs shape the water balance and productivity patterns of most dry regions of the world (Noy-Meir, 1973). However, arid lowlands flanked by high water yield areas, such as mountain ranges or humid highlands, can receive extra water inputs through rivers and aquifers. These lateral water supplies often sustain irrigated and natural oases, i.e., riparian and phreatophytic ecosystems – also termed termed inflow dependent ecosystems (IDEs) (Van Dijk, 2010) – of high evapotranspiration, productivity, diversity, and economic importance (Ezcurra, 2006; Kingsford, 2006). The magnitude, fate, and human influence on these water supplies are key to understanding and managing arid lands.

Some of the largest desert irrigated oases of the world rely on water supplied by large rivers from adjacent mountain ranges. Example of these are the cases of the Indus river conveying water from the Himalayas range to the Punjab lowlands in India and Pakistan (17 Mha according to Siebert et al., 2007); the Euphrates-Tigris rivers delivering water from the Kargapazari and Taurus mountains to the Syrian and Arabian deserts (4 Mha, Siebert et al., 2007); or the rivers born in the Kunlun, Pamir and Tian Shan mountains supplying the Taklamakan desert in China (1 Mha, Siebert et al., 2007). In the Americas, several irrigated areas lay at both sides of the Rocky–Andes ranges with the Colorado River (US), Maipo–Aconcagua (Chile) and, San Juan–Mendoza–Tunuyán

* Corresponding author. Present address: Department of Soil and Water Conservation, Centro de Edafología y Biología Aplicada del Segura, Consejo Superior de Investigaciones Científicas, Murcia, Spain.
*E-mail address:* scontreras@cebas.csic.es (S. Contreras).

0022-1694/$ - see front matter © 2010 Elsevier B.V. All rights reserved.
doi:10.1016/j.jhydrol.2010.11.014

(Argentina) systems feeding some of the largest oases. Mountain water supplies are not restricted to irrigated arid lands but also include natural inflow dependent ecosystems (riparian and floodplain-phreatophytic oases), where ET is increased due to lateral water inflows. Water supplies from mountain ranges to deserts are not only conveyed by rivers but also by aquifers. For example, the Great Artesian Basin covering ~20% of the Australian continent encompasses largely arid landscapes (Simpson, Tirari and Strzelecki deserts) to the west of the Great Dividing Range. This large groundwater reservoir supports a multitude of wetland ecosystems of high ecological and economic value (Cox and Barron, 1998). The identification of inflow dependent ecosystems is being focus of special interest in the last years (Howard and Merrifield, 2010; Brown et al., 2010), yet the extent and magnitude of the water supplies to these areas and their trade-off with irrigation has been poorly quantified (Cai et al., 2003; Tao et al., 2009).

Human activities may impact the regional water balance of arid regions that receive mountain water supplies in two main ways: (1) directly by intercepting and diverting water supplies away from their original pathways and sinks towards irrigated areas and (2) indirectly by introducing disturbances such as grazing, logging or burning that alter local water fluxes. In both cases the water balance and primary productivity across the region can be affected and trade-offs among productive systems (e.g. dryland vs. irrigated farming) or ecosystem outputs to society (e.g. food production vs. biodiversity conservation) can emerge (Ezcurra, 2006). A prime example of these trade-offs has been the fast development of irrigation in the Aral Basin (Glantz, 1999; Cai et al., 2003). The Aral sea was the fourth largest lake in the world in 1960, however, its volume has been reduced by 80% and its area by 60% by 2000s because of the diversion of $\sim 110\ km^3\ y^{-1}$ of water from the Amu Darya and Syr Darya rivers to irrigate more than 4 Mha along their middle and lower sections in Turkmenistan, Uzbekistan and Kazakhastan (Cai et al., 2003; Siebert et al., 2007). Overexploitation of these rivers not only led to rapid drying of the original sink, but also caused other environmental and ecological problems such as water quality degradation, waterlogging, and soil erosion and salinization (Glantz, 1999; Hillel, 2000), which have been common throughout the history of irrigation across many artificial oases (Hillel, 2000).

Because evapotranspiration (ET) constitutes the most important water balance component in arid and semiarid regions, the accurate knowledge of its magnitude and spatial pattern is essential for sustainable water and land resource management. Remote sensing offers a suitable mean for monitoring land surface attributes that are directly involved in the exchange of water throughout the soil–plant–atmosphere continuum (SPAC) (Glenn et al., 2007; Kalma et al., 2008; Godwa et al., 2008). Evapotranspiration rates from satellite data can be retrieved from: (a) physically-based algorithms which aim to compute ET directly from the application of the Penman–Monteith equation (Cleugh et al., 2007; Mu et al., 2007; Zhang et al., 2008, 2009) or the complementary relationship (Venturini et al., 2008), or indirectly from a *residual approach* once the rest of the surface energy balance components are quantified (see review by Kalma et al., 2008); (b) surface temperature/vegetation index ($T_s$/VI) methods, also called triangle-trapezoidal methods, which compute an evaporative coefficient from the spatial analysis of the $T_s$–VI scatterplot domain (see review by Petropoulos et al., 2009) and (c) numerical or process-based methods based on Soil–Vegetation–Atmosphere (SVAT) models or Land Surface Models (LSMs) which simulate the continuous and hourly transfer of heat and water in the SPAC when they are driven by weather and radiation data (Pitman, 2003).

Physically-based algorithms resting on the residual approach provide instantaneous-daily estimates of ET but they require ground-based data and a large parameterization to compute the surface energy balance from satellite data. In a recent paper, Sun et al. (2009) reduce the requirements of ground data but even so, residual methods are still difficult to be operative and scaled-up in getting coarser spatial scales (regional–global) and temporal resolutions (seasonally–yearly). Despite Penman–Monteith-based models developed in the last years have simplified the model structure and parameterization with respect to residual methods, they continue to be dependent on meteorological (humidity and wind speed) and auxiliary (vegetation height and length roughness) data which are often not available. The estimation of the evaporative fraction using $T_s$/VI methods is subjected to some empiricism and user subjectivity in determining the wet and dry boundaries of the $T_s$/VI scatterplot, being the uncertainties higher as coarser is the image resolution (Kalma et al., 2008; Petropoulos et al., 2009). Finally, numerical models are usually very complex in their internal structure being sometimes subjected to equifinality problems associated with overparameterization issues (Kalma et al., 2008).

A more critical issue in complex arid and semiarid regions results from the lack of effective means to verify satellite-based ET outputs at scales greater than few kilometres (McCabe and Wood, 2006; Kalma et al., 2008). Besides their high acquisition and maintenance costs, ground-based flux measurements derived from Bowen ratio and eddy covariance systems have an uncertainty of 20–30% or even higher when no representative areas are covered or the calibration procedure is not adequate (Kalma et al., 2008 and references therein). A similar 10–30% range of error has been reported when satellite-based daily ET estimates are compared against ground-based ET measurements (Jiang et al., 2004). At coarser scales when no direct ET measurements exist, comparison of ET values derived from classical water budget balance approaches or the analysis of ET fields derived from different LSMs provide good opportunities to evaluate satellite-based ET estimates at landscape and regional scales (Zhang et al., 2008; Guerschman et al., 2009). Nowadays, an algorithm that achieves the right balance between accuracy and simplicity is still missing (Cleugh et al., 2007).

Evapotranspiration models based on ecological assumptions emerge as a potential alternative to physically-based algorithms with high parameterization requirements, and $T_s$/VI methods that are highly context-dependent and therefore difficult to extrapolate. In natural water-limited ecosystems, the balance between rainfall and plant water use follows an optimization pattern in which evapotranspiration is maximized and non-evapotranspirative water losses (recharge and runoff) are minimized (Specht, 1972; Eagleson, 1982; Hatton et al., 1997; Rodríguez-Iturbe and Porporato, 2004). As a result, evapotranspiration increases linearly with rainfall and only exceeds expected rainfall-based values if additional water resources are available. The linear increase of evapotranspiration with precipitation is associated with higher canopy conductances, mainly driven by growing leaf area indexes (Kelliher et al., 1995). Our model relies on the fact that the light (photosynthetically active radiation) absorption of canopies, which is strongly associated to leaf area, can be remotely characterized by radiometric vegetation indexes (Gamon et al., 1995; Glenn et al., 2008 and references therein). Quantifying and mapping deviations of vegetation indexes from expected precipitation-based values could then provide insights into the magnitude and distribution of both water supplies (positive anomalies) and suboptimal water consumption (negative anomalies) related to degradation or substrate limitations (Prince et al., 1998; Boer and Puigdefábregas, 2005) as well as recharge opportunities (Contreras et al., 2008).

In this paper we introduce an ecological satellite-based model to identify IDEs and retrieve annual and seasonal evapotranspiration fields in arid and semiarid regions based on the assessment of the Enhanced Vegetation Index (EVI), its relationship with

precipitation, and the departures from this relationship (EVI anomalies) associated with additional surface and ground water contributions to natural and irrigated ecosystems (evapotranspiration anomalies). We evaluate the model in the central sector of the Monte desert in Argentina, where the major irrigated oases of South America are found, by contrasting our ET estimates with those retrieved independently from: (A, plot scale) known evapotranspiration coefficients for non-stressed irrigated crops and rainfed grassland/pastures (Allen et al., 1998), (B, basin scale) water budgets computed for three irrigated oases using river flow and irrigation statistics. Finally, the imprint of Andean water contributions on the maintenance of inflow dependent ecosystems and their water balance is discussed.

## 2. Material and methods

### 2.1. Satellite-based evapotranspiration estimates: an ecological approach

We developed an ecological approach that estimates evapotranspiration (ET) at an annual scale based on the positive and linear relationship between the water inputs received by ecosystems, their capacity to capture light, and their evapotranspiration rates as suggested by the hydrological equilibrium hypothesis (Nemani and Running, 1989). According to this hypothesis, absorbed photosynthetically active radiation, strongly related with the leaf area index (LAI) and easily captured by remotely sensed vegetation index (EVI), approaches an equilibrium with mean precipitation inputs in areas that are not disturbed and have no substrate constraints to plant growth (factors leading to lower than expected EVI) and receive no additional water supplies (factor leading to higher than expected EVI) (Fig. 1A). In dry ecosystems this equilibrium implies an exhaustive use of precipitation and hence a linear association of EVI and evapotranspiration to precipitation. Support for the precipitation-EVI positive linear relationship, developed theoretically by Eagleson (1982), comes from field studies (Specht, 1972; Lo Seen Chong et al., 1993; Eamus, 2003; Emanuel et al., 2007; Ellis and Hatton, 2008), model simulations (Eagleson, 1982; Nemani and Running, 1989) and remote sensing exercises (Jobbágy et al., 2002; Del Grosso et al., 2008). On the other hand, the EVI–ET relation is supported by the positive linear relationship displayed between LAI and annual evapotranspiration rates within water-limited environments (Greenwood et al., 1985; Nemani and Running, 1989; Hoff et al., 2002; Groeneveld et al., 2007). Following the hydrological equilibrium hypothesis, the ecological model developed here proposes that the positive anomalies between observed EVI values and those expected from precipitation are proportional to the actual consumption of supplementary water sources (i.e. direct use of phreatic groundwater, natural surface water contributions, irrigation), whereas negative anomalies are proportional to the fraction of precipitation inputs that are not consumed by vegetation and are lost as surface runoff, deep drainage or excessive direct evaporation (more than what is commonly lost through this pathway at a given precipitation level). As consequence, evapotranspiration anomalies are defined in this study as the evapotranspiration rates in excess or deficit of precipitation supply.

Guided by the previous reasoning and considering that optimization patterns in water use are better explained when long temporal periods are taken, we established a linear relationship between EVI and the local precipitation at a mean annual timescale as shown by the following equation (see dashed line in Fig. 1A)

$$EVI_{map} = a\,\mathrm{MAP} + b \quad (1)$$

where $EVI_{map}$ is the precipitation-based EVI, MAP is the mean annual precipitation and, $a$ and $b$ are fitted-parameters computed regionally following an empirical approach based on a quantile regression analysis. With this approach we are able to estimate the expected EVI value for a vegetation cover that exclusively uses local precipitation and is in equilibrium with long-term

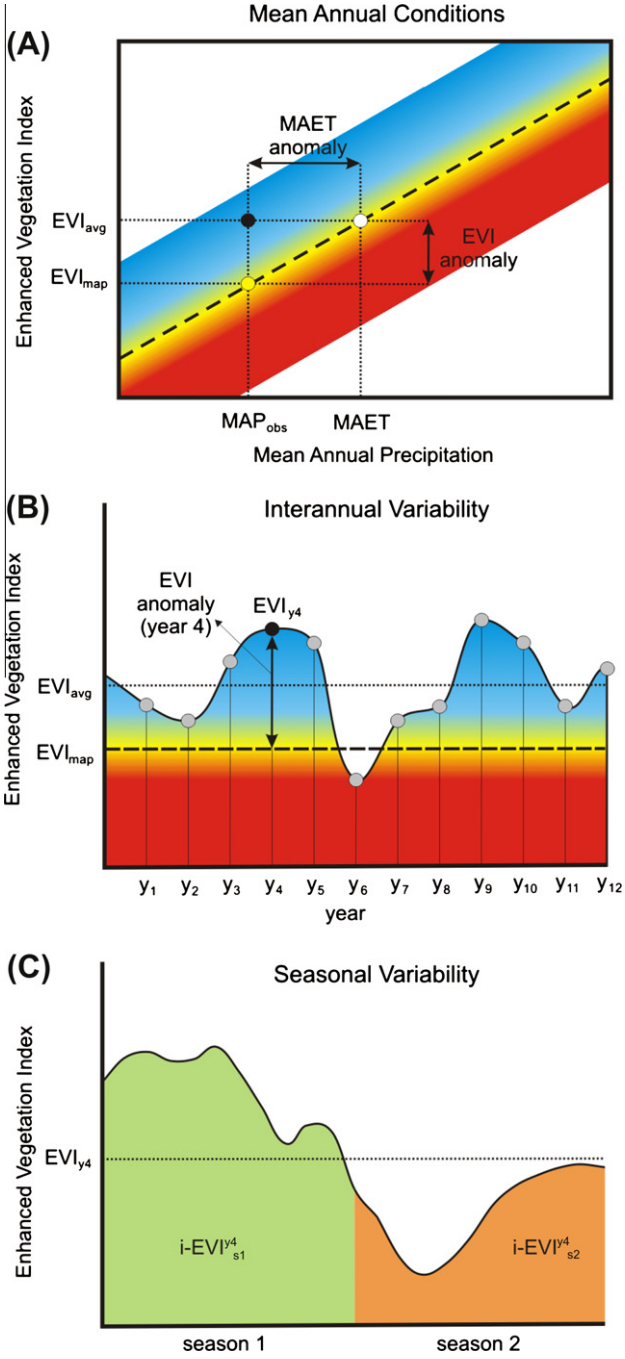


**Fig. 1.** Conceptual downward approach to estimate annual/seasonal evapotranspiration rates. (A) A MAP–EVI relationship (dashed line) is regionally calibrated for estimating $EVI_{map}$ values for a given annual precipitation and from which mean annual EVI and ET anomalies are computed. Mean annual evapotranspiration (MAET) for an observed "average" EVI ($EVI_{avg}$, black circle), is expected to be equal to the mean annual precipitation that would be required to support the observed EVI if the vegetation was at equilibrium with the local precipitation (white circle). (B) Annual evapotranspiration estimates are computed from year-by-year EVI anomalies (differences between annual average EVI and $EVI_{map}$). (C) Annual ET estimates are seasonally scaled according to the accumulated EVI value ($i$ – EVI) computed in each season period. Blue and red shades in (A) and 9B) are referred to positive and negative EVI anomalies regarding to the precipitation-based EVI ($EVI_{map}$, in yellow shade), respectively. (For interpretation of the references to colour in this figure legend, the reader is referred to the web version of this article.)

precipitation (Boer and Puigdefábregas, 2003). The regional MAP–EVI function provides us with the EVI value ($EVI_{map}$) for which annual ET is approached to the mean annual precipitation. At annual timescale, we defined the concept of *EVI anomaly*, as

$$\text{EVI anomaly} = EVI_{yX} - EVI_{\text{map}} \quad (2)$$

where $EVI_{yX}$ is the observed annual average of EVI in the year X computed from satellite images (Fig. 1A). At those pixels in which vegetation is in hydrological equilibrium, i.e. $EVI_{yX} = EVI_{map}$, annual evapotranspiration is expected to be equal to MAP. Using Eq. (1), total evapotranspiration rate for a given year can be approach from its average EVI (Fig. 1B) as

$$ET_{yX} = \frac{EVI_{yX} - b}{a} \quad (3)$$

where $ET_{yX}$ is estimated as the MAP required to sustain the observed EVI value in the year *X*. Similarly to EVI, we can now define the mean annual ET anomaly in the year *X* that will be positive if $EVI_{yX} > EVI_{map}$, or negative if $EVI_{yX} < EVI_{map}$

$$\text{ET anomaly} = ET_{yX} - \text{MAP} \quad (4)$$

The yearly ET anomaly could be equally defined using Eq. (4) when $ET_{yX}$ and MAP are substituted by the annual ET and precipitation values respectively

Rearranging Eqs. (1)–(4), we state

$$\text{ET anomaly} = \frac{1}{a}\ \text{EVI anomaly} \quad (5)$$

Positive evapotranspiration anomalies suggest that other water sources, in addition to precipitation, contribute to the capacity of the canopy to absorb light and to generate green biomass, whereas negative anomalies indicate that a fraction of precipitation escapes from vegetation consumption, returning to the land as runoff or recharging aquifers as deep drainage.

Finally, annual ET estimates can be seasonally scaled for sufficiently long periods in order to reduce the lag usually observed between ET and vegetation activity in drylands according to the seasonal integrated EVI ($i - \text{EVI}$) (Fig. 1C) as

$$ET_{sZ}^{yX} = ET_{yX}\frac{i - EVI_{sZ}^{yX}}{i - \text{EVI}_{yX}} \quad (6)$$

Being $i - \text{EVI}$ the total EVI accumulated during the season (numerator) and all year (denominator). Scripts *yX* and *sZ* are refereed to the year *X* and season *Z*, respectively.

In this approach, the response of EVI–MAP, and therefore the response of evapotranspiration to MAP, was assumed invariant across vegetation types as partially supported by the field data collected by Schulze et al. (1994) and Kelliher et al. (1995) who showed that the maximum surface conductance of most global vegetation types generally fall within a very narrow band of values. This assumption is also supported by field estimates of primary productivity, closely coupled with transpiration (Monteith, 1988), which showed a linear relationship between annual rainfall and primary productivity across a broad range of vegetation types (from deserts to dense forests) (Austin and Sala, 2002; Knapp and Smith, 2001).

### 2.2. Study region

The study region encompasses an area of 87,500 km$^2$ of lowlands ($\leqslant$1000 m a.s.l.) and expands over the Central Monte desert in Argentina between 31°S and 36°S (Fig. 2). The Andes Cordillera and the Sierras Pampeanas constitute the western and eastern boundaries of the region, respectively. As a general pattern, snowfields along more than 800 km of mountain front in the Cordillera range (elevation = 2400–7000 m) feed streams that converge into six major rivers, from north to south: Jachal-Bermejo, San Juan, Mendoza, Tunuyan, Diamante and Atuel. After crossing the Precordillera range (elevation = 1000–4300 m) these rivers reach alluvial fans and sedimentary plains of the Central Monte desert to finally discharge into the Desaguadero–Salado river system (Fig. 2). Precipitation inputs in the high Cordillera and Central Monte lowlands have contrasting moisture sources and seasonalities. In the central Cordillera, precipitation is derived from Pacific Ocean moisture and occurs mostly as snow. It is concentrated in the cold season (May–October) and ranges from 400 to 900 mm y$^{-1}$ (Abraham and Rodríguez, 2000). In the Central Monte lowlands precipitation is mainly associated with convective storms that occur during the warm season (November–April), ranging from 150 to 400 mm y$^{-1}$ and being fed by the Atlantic Ocean and continental moisture sources (Abraham and Rodríguez, 2000). Mean annual temperature in the Central Monte ranges from 13 to 19 °C and potential ET, according to the FAO-Penman–Monteith equation, reaches values close to 1400 mm y$^{-1}$ in the driest parts of the study region. A detailed review of the main biophysical and socio-economic characteristics of the Monte desert is given by Abraham et al. (2009), while Villagra et al. (2009) review some of the effects that land use and disturbance factors have had on the dynamics of the natural ecosystems of the desert.

Andean rivers are the main sources of water for the largest irrigated system of South America with 0.17 Mha (Departamento General de Irrigación, 2004a). Four large artificial oases are located in the region (Fig. 2, Table 1), with vineyards, olives, and fruit trees being the main crops. These oases assemble ~90% of the economic activity in the region and more than 1.5 million people live there (Table 1). The value added to the regional economy by the agricultural sector represents 35% (Departamento General de Irrigación, 2004b). Furrow, flood and, to a lesser extent, drip irrigation, are the most usual irrigation techniques. Conveyance and water distribution systems in all irrigated oases are also characterized by large inefficiencies (Departamento de Irrigación, 2004b). Downstream of artificial oases and their associated human settlements, landscapes are dominated by sandy plains of fluvial, lacustrine and eolian origin with widespread dune fields (Abraham et al., 2009). Open woodlands of *Prosopis flexuosa* occupy the inter-dune depressions, where groundwater levels are relatively shallow ($\leqslant$10 m depth). The best examples of those phreatophytic woodlands are sparsely distributed in the rangelands of the Guanacache Plain (~100,000 Mha; Fig. 2) (González-Loyarte et al., 2000; Jobbágy et al., 2010). The floodplains of the main Andean rivers host marshes and wetlands with the Rosario–Guanacache lagoon system, at the confluence of the San Juan, Mendoza and Jachal-Bermejo rivers, being the largest wetland of the region. Both, open woodlands and wetlands, supply key ecological services and resources for the survival of local economies (Villagra et al., 2009).

Groundwater is the third source of water for natural ecosystems and irrigated areas in the Central Monte desert after surface water inflows from Andean rivers and local precipitation (Departamento General de Irrigación, 2004b; Jobbágy et al., 2010). Major detritic aquifers are phreatic at the apical and middle sections of the alluvial fans, becoming increasingly confined downslope. The average saturated thickness ranges from 100 to 400 m, with storage coefficients of 0.10–0.15 for the Mendoza aquifers and 0.35 for the aquifer underlying the San Juan oasis (Abraham and Rodríguez, 2000). Recharge takes place as seepage in the stream beds of the apical areas of alluvial fans and in the conveyance systems of irrigated lands (Abraham and Rodríguez, 2000; Departamento General de Irrigación, 2004b).

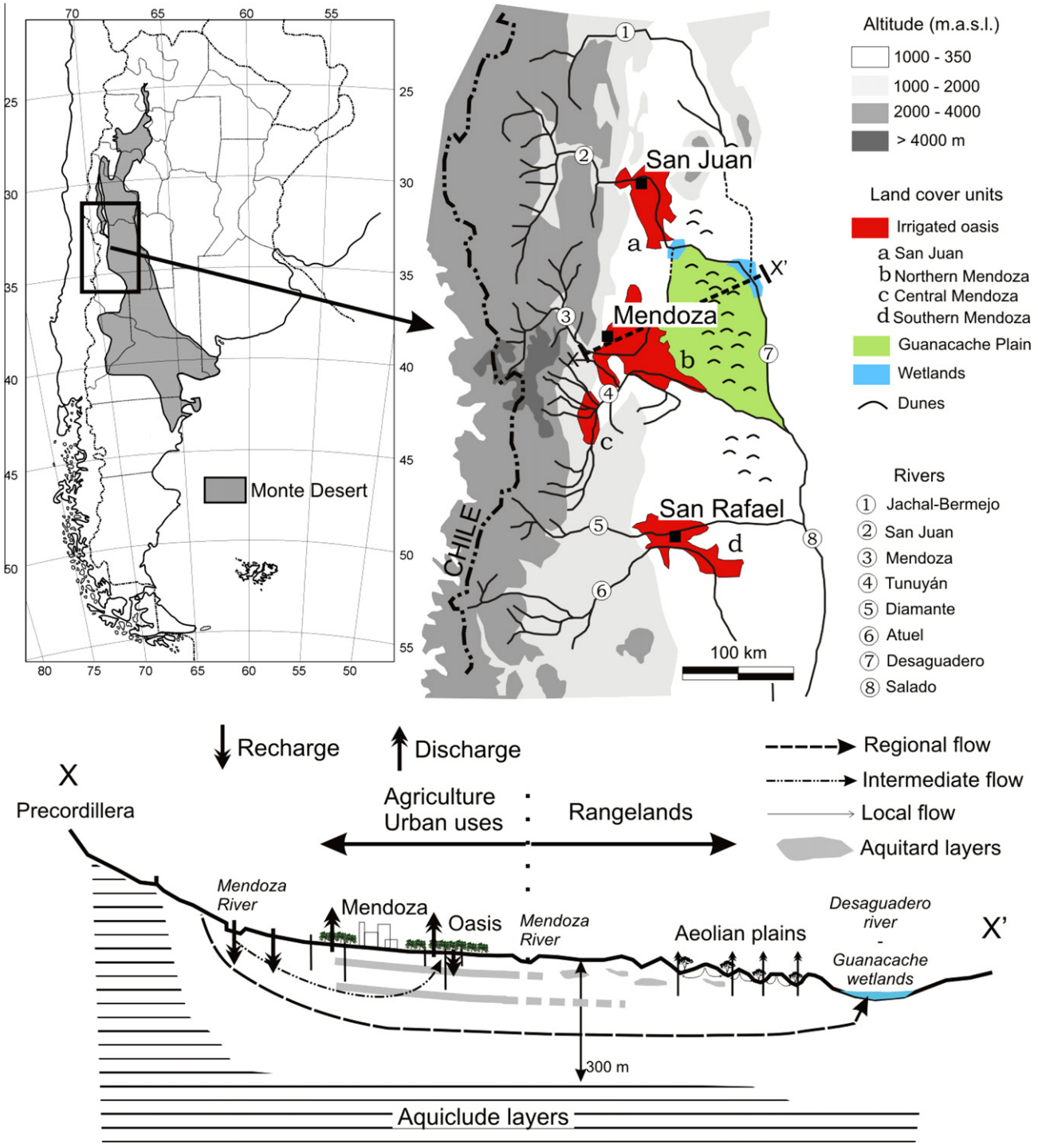


**Fig. 2.** Location map showing the extension of the Monte desert in Argentina, the main land cover types in the region and a non-scaled conceptual *W–E* transect and water fluxes model (indicated by the *X–X'* line) with the most important landscape features of the area.

### 2.3. Climate and satellite data

The CRU CL 2.0 dataset (New et al., 2002) was used to compute mean monthly maps of precipitation and potential evapotranspiration. This database was elaborated by the UK Climate Research Unit for the 1961–1990 period and has a spatial resolution of 10 min (~18 km). Maps were generated for a window of 1100 × 1100 km, fitting with the size of the MODIS tile which covers the study region. An ordinary kriging interpolation algorithm was applied for this window to resample original maps from a 10 min to a 250 m spatial resolution. Mean annual precipitation (MAP) values computed from the CRU dataset ($MAP_{CRU}$) were finally cross-validated and locally corrected ($MAP = -47.198 + 0.996\ MAP_{CRU}$; $R^2 = 0.95$) with 66 MAP values extracted from: (a) meteorological stations in the CLIMWAT 2.0. database ($n = 33$; FAO, 2006) and (b) technical documents with data referred to another 33 meteorological stations located in the driest areas of the Central Monte desert (Le Houréou, 1999 and references therein). MAP values from CLIMWAT data and local meteorological stations were assumed to be broadly representative of the 1961–1990 period (all average figures are referred to periods of

**Table 1**
Main characteristics of the artificial oases in the study region. Population corresponds to the 2001 census (INDEC, 2001). Average annual river flows and discharges correspond to gauge stations located upstream the boundaries of the artificial oases (Subsecretaría de Recursos Hídricos, 2004). Data in the last column show the volume of total (and exploitable) groundwater reserves in the aquifers underlying each oasis (Abraham and Rodríguez, 2000).

| Oasis | Population (inhab.) | Cultivated area (ha) | Major crops | Rivers (flow $m^3/s$, discharge $hm^3\ y^{-1}$) | Aquifers ($hm^3$) |
|---|---|---|---|---|---|
| San Juan | 421,640 | 89,103 | Wine grapes<br>Olives | San Juan<br>65.2/2059 | 135,000<br>(7800) |
| Northern Mendoza | 848,660 | 178,147 | Wine grapes<br>Vegetables | Mendoza<br>45.0/1420<br>Lower Tunuyán<br>32.6/1024 | 228,000<br>(6480) |
| Central Mendoza | 42,125 | 92,792 | Fruit trees<br>Vegetables | Upper Tunuyán<br>28.8/898[a] | 96,000<br>(4800) |
| Southern Mendoza | 184,568 | 70,765 | Fruit rees<br>Olives | Diamante<br>40.0/1262<br>Atuel<br>34.7/1096 | 135,000<br>(4050) |

[a] 492 $hm^3\ y^{-1}$ are additionally supplied by different streams and creeks.

more than 15 years covering at least 2/3 of the CRU normal period). The local correction of the CRU dataset was required because of inconsistencies initially observed between original $MAP_{CRU}$ values and the long-term average precipitation values measured in the driest areas of the region. Observed mean annual precipitation for three meteorological stations located in the region along a *N–S* transect (San Juan, Tres Porteñas–Mendoza and La Llave–San Rafael) for our study period (2001–2006) was only 4% below CRU values (149 vs. 155 mm $y^{-1}$), indicating that this database was appropriate as a reference in that temporal span.

The Enhanced Vegetation Index (EVI) MOD13Q1 land product from MODIS Collection 4 (Huete et al., 2002) was extracted for the period 2001–2006. EVI, which combines data from the blue, red and infrared spectral bands, was preferably used than NDVI for its higher sensitivity in high biomass situations, and because atmospheric interferences and soil background signal are more effectively removed (Huete et al., 2002). Additionally, EVI has been proved to be more suitable in estimating ET than NDVI (Nagler et al., 2005). Because at the beginning of this study, collection 5 of MODIS products was not launched yet, a comparison of EVI values from collection 4 and 5 was performed for the 2003 year. For this purpose, we randomly selected 1440 pixels in the study area and we computed the average EVI values for the study year. The statistical analysis showed minimal differences between both collections (Mean $EVI_{coll\ 4} = 0.129$; Mean $EVI_{coll\ 5} = 0.127$; $R^2 = 0.98$; RMSE = 0.019; $n = 1440$), which would suggest that no significant changes in the final results would be obtained if we use the new collection instead of collection 4.

Based on the general seasonal pattern of EVI observed in the region, two periods of different vegetation activity were defined for scaling annual ET estimates: a growing season period from October to April and a "dormant" season period from May to September.

### 2.4. Model calibration and application

Eq. (1) was parameterized across 125 reference sites that meet the criteria of having low disturbance rates and lacking natural or artificial water supplies, as confirmed by field inspection, existing vegetation maps, digital elevation models and high-resolution satellite images (Quickbird images in the Google Earth system). Although all these reference sites were located in flat areas with confirmed deep groundwater levels and away from hillslopes or surface water pathways that could contribute with run-on waters, we used the 75th-quantile regression of mean annual EVI (2001–2006) vs. MAP as a conservative value to generate $EVI_{map}$ values under broad precipitation conditions. Blossom software (Cade and Richards, 2005) was used to extract the 75th-quantile regression model for the reference sites selected. Because this threshold quantile is a key parameter in our approach, we performed an analysis to test the sensitivity of annual ET estimates to changes in the quantiles used. Negligible impacts on the slope and constant fitted-parameters were found when different quantiles values were chosen (data not shown), ranging between $3.31–3.09 \times 10^{-4}$ and 0.063–0.093 for the 50th- and 95th-quantile values.

Based on our whole region analysis we identified contrasting land cover types for which EVI and ET anomalies were computed. With the aid of high spatial resolution images (Quickbird – Google Earth system) we selected a collection of individual sites representing wetlands and riparian communities ($n = 10$), groundwater-fed woodlands ($n = 10$), salty flats and lowlands ($n = 10$), semi-active bare dunes ($n = 10$), non-salinized irrigated croplands ($n = 40$, $n = 10$ for each major irrigated oases) and salinized irrigated croplands ($n = 10$ with sites located at the San Juan and Northern Mendoza oases). All selected sites covered a surface area of 1 $km^2$ which corresponds to a window of $4 \times 4$ MODIS pixels. Natural and irrigated salt-affected areas were identified by the presence of surface salt accumulation signs. Basic statistics (means and standard errors) for all the variables used in the study (MAP, observed EVI, EVI and ET anomalies) were computed for each land cover type, and statistical differences among them were assessed using ANOVA analyses and post hoc Tukey tests.

### 2.5. Model evaluation

#### 2.5.1. Crop coefficient approach

Evapotranspiration estimates from Eq. (3) were compared with values obtained after computing Penman–Monteith reference evapotranspiration and applying typical crop coefficients reported in the literature (Allen et al., 1998) for olive ($k_{c\_annual\ average} = 0.60$), wine grape ($k_{c\_annual\ average} = 0.40$), and grassland/pastures ($k_{c\_annual\ average} = 0.44$) located in the driest and wettest areas of the study region, respectively. Annual evapotranspiration based on the crop coefficient approach, $ET_{FAO}$, was computed as:

$$ET_{FAO} = \sum_{i=1}^{12} ET_{0,i}\, x\ k_{c,i} \tag{7}$$

where $ET_0$ is the monthly reference evapotranspiration from the FAO-Penman–Monteith equation (Allen et al., 1998), $k_c$ is the crop coefficient corresponding to month *i*. Monthly $k_c$ values were obtained (Eq. (8)) by scaling the annual maximum and minimum $k_c$ values reported by FAO (Allen et al., 1998) according to the annual maximum and minimum EVI values observed for each vegetation cover:

$$k_{c,i} = \frac{(EVI_i - EVI_{\min})\ (k_{c,\max} - k_{c,\min})}{(EVI_{\max} - EVI_{\min})} + EVI_{\min} \tag{8}$$

*2.5.2. Water budget approach*

A second testing of the model involved watershed level values for three irrigated oases for which regional irrigation budgets could be established. In each oasis we compared and integrated estimates of ET anomalies based on 250 randomly selected sites with those derived from the following water mass balance:

$$WBA_{irrig} = \frac{10^5}{S_c}\{[D - UI_F] \cdot \Gamma_{cds} \cdot \Gamma_{fa} + [P - UI_{GW}] \cdot \Gamma_{fa}\} \quad (9)$$

where $WBA_{irrig}$ is the depth of water that is effectively consumed by artificial oasis besides annual precipitation (mm $y^{-1}$), $S_c$ is total cultivated area (ha), $D$ and $P$ are the annual water volumes diverted from rivers and aquifers, respectively ($hm^3\ y^{-1}$) and $UI$ is the volume of water used to satisfy urban and industrial demands ($hm^3\ y^{-1}$) derived from rivers (subindex $F$) and aquifers (subindex GW). Finally, $\Gamma_{cds}$ and $\Gamma_{fa}$ represent the efficiency of conveyance/distribution and application systems at the plot, respectively. $S_c$ values for each oasis were obtained from Landsat imagery in 2001 (Departamento General de Irrigación, 2004a), while the remaining data were collected from Basin Water Management Plans developed by the Regional Irrigation Bureau of Mendoza (Departamento General de Irrigación, 2004b).

## 3. Results

Vegetation greeness (mean annual EVI) increased linearly with precipitation (MAP) across reference sites, providing an effective ($EVI_{map}$ = 0.066 + 3.5 × $10^{-4}$ MAP; $R^2$ = 0.91, $p$ < 0.01, Fig. 3) background function from which the distribution and magnitude of EVI and associated ET anomalies could be computed and mapped (Fig. 4). While most of the region displayed a widespread pattern of slightly negative EVI anomalies (71% of the area), clusters of highly positive EVI anomalies (29% of the area) were especially evident in the driest portion of the region (Fig. 4A, B and C). Integrated across the whole region, positive and negative EVI anomalies are almost balanced having a small average (±standard error) negative value of −0.0030 ± 0.0001.

Positive EVI anomalies were more intense in artificial oases, where irrigation is a common practice. Covering almost 10,000 $km^2$ (11% of the study region), artificial oases hosted 38% of the area with positive anomalies but 79% of the total accumulated EVI anomalies in the entire region. More than 75% of the area in the artificial oases showed EVI anomalies greater than 0.05. The spatially-aggregated mean annual evapotranspiration (MAET) estimated for all oases was 4505 $hm^3\ y^{-1}$ (470 mm $y^{-1}$) accounting for a total ET anomaly of 2815 $hm^3\ y^{-1}$ (295 mm $y^{-1}$), i.e. 1.7 times more water than the total volume supplied by precipitation.

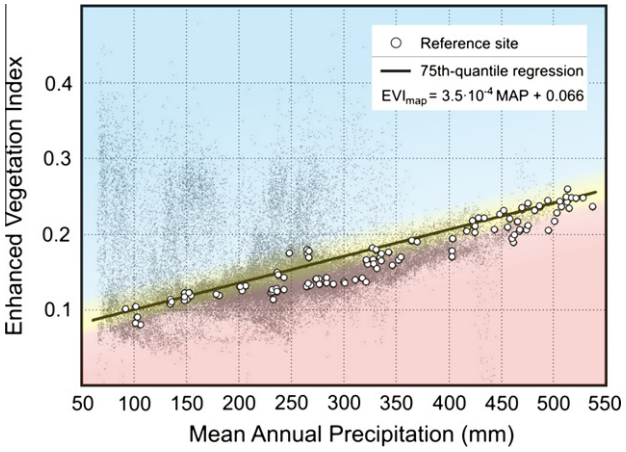


**Fig. 3.** Regional MAP–EVI model function calibrated for the Monte Desert. The solid black line corresponds to the 75th-quantile regression fitted from a total of 125 reference sites (open circles). Small grey-circles are a random sample of pixels with a runoff topographic index equal to 1 (i.e. no run-on inputs). As in Fig. 1, blue and red shades define the dual-domain of positive and negative EVI–ET anomalies, respectively.

Positive EVI anomalies in natural systems were linked to wetlands and riparian communities and groundwater-fed woodlands close to the main course of the Andean rivers or in landscape sections with shallow water tables (Fig. 4A and B). Although the total area with positive EVI anomalies, i.e. inflow dependent ecosystems, covered 63% of the region (15,900 $km^2$), their accumulated ET anomaly was 770 $hm^3\ y^{-1}$ (∼50 mm $y^{-1}$), equivalent approximately to one fourth of what we computed for artificial oases (Fig. 4A and B).

Negative EVI anomalies were generally located on the eastern side of the study region, being more extreme in the driest lowlands surrounding the Guanacache wetlands and the Jachal-Bermejo and Desaguadero rivers. Moderate values were also found in the corridors located between the Tunuyán, the Diamante and the Atuel rivers, areas that have been degraded by vegetation fires and overgrazing during the past few decades (Villagra et al., 2009). Covering an area of 62,100 $km^2$, natural vegetation with negative EVI anomalies, accounted for −4400 $hm^3\ y^{-1}$ (−70 mm $y^{-1}$) of accumulated ET anomalies. Excluding urban areas, the area with negative EVI anomalies in the artificial oases was estimated in 290 $km^2$ (3% of artificial oases area) but the associated accumulated ET anomaly reached only −13 $hm^3\ y^{-1}$ (−45 mm $y^{-1}$).

Among the natural inflow dependent ecosystems, riparian and wetlands communities showed the highest positive EVI anomalies (Table 2). Mean annual EVI observed in wetlands was, on average, more than twice their precipitation-based expected values. According to their EVI anomalies, the mean (±standard error) values of annual evapotranspiration estimated for wetlands was 672 (±50) mm $y^{-1}$, or 3.1–3.4 times the MAP of those sites. For wetlands, annual evapotranspiration during the period 2001–2006 ranged from 346 to 842 mm $y^{-1}$ (Fig. 5), accounting the growing season period for 69% of the mean annual ET (Table 2). In contrast to wetlands, observed EVI values in groundwater-fed woodlands were only 10% higher than their precipitation-based expected values, suggesting that the EVI values observed in these ecosystems are close to their hydrological equilibrium values. Evapotranspiration losses in these areas were in the 166–203 mm $y^{-1}$ range, accounting the growing season period for 61% of the mean annual ET. According to the slight positive EVI anomalies observed in these woodlands (Table 2), the mean annual rate of groundwater consumption by them would approach 39 mm $y^{-1}$ or 1.25 times the local rainfall.

Salty areas in lowlands and fields of semi-active dunes showed the lowest EVI (0.08–0.09). In non-salinized irrigated croplands, observed EVI values were slightly lower than in wetlands but 1.75 times higher than in dunes and salty areas (Table 2). Estimates of evapotranspiration during the 2001–2006 period ranged from 45 to 96 mm $y^{-1}$ for dunes sites, and from 31 to 55 mm $y^{-1}$ for salty areas. Seasonal evapotranspiration during the growing period was similar in both land cover types, accounting in average for 56% of the total annual evapotranspiration. The impact of salinization in irrigated croplands promoted an average reduction of 30% in the observed EVI values. Although still positive, EVI and ET anomalies in salinized irrigated croplands were only 0.07 and 210 mm $y^{-1}$, respectively. These values were ∼45% less than those calculated for croplands that were not affected by salts accumulation.

Satellite-based mean annual evapotranspiration estimates for irrigated wine grapes and olives in the Northern Mendoza oasis, and grasslands/pastures in the wettest edge of the study matched well with values retrieved through the crop coefficient approach (Fig. 6). No significant differences ($p$ < 0.01) were found between

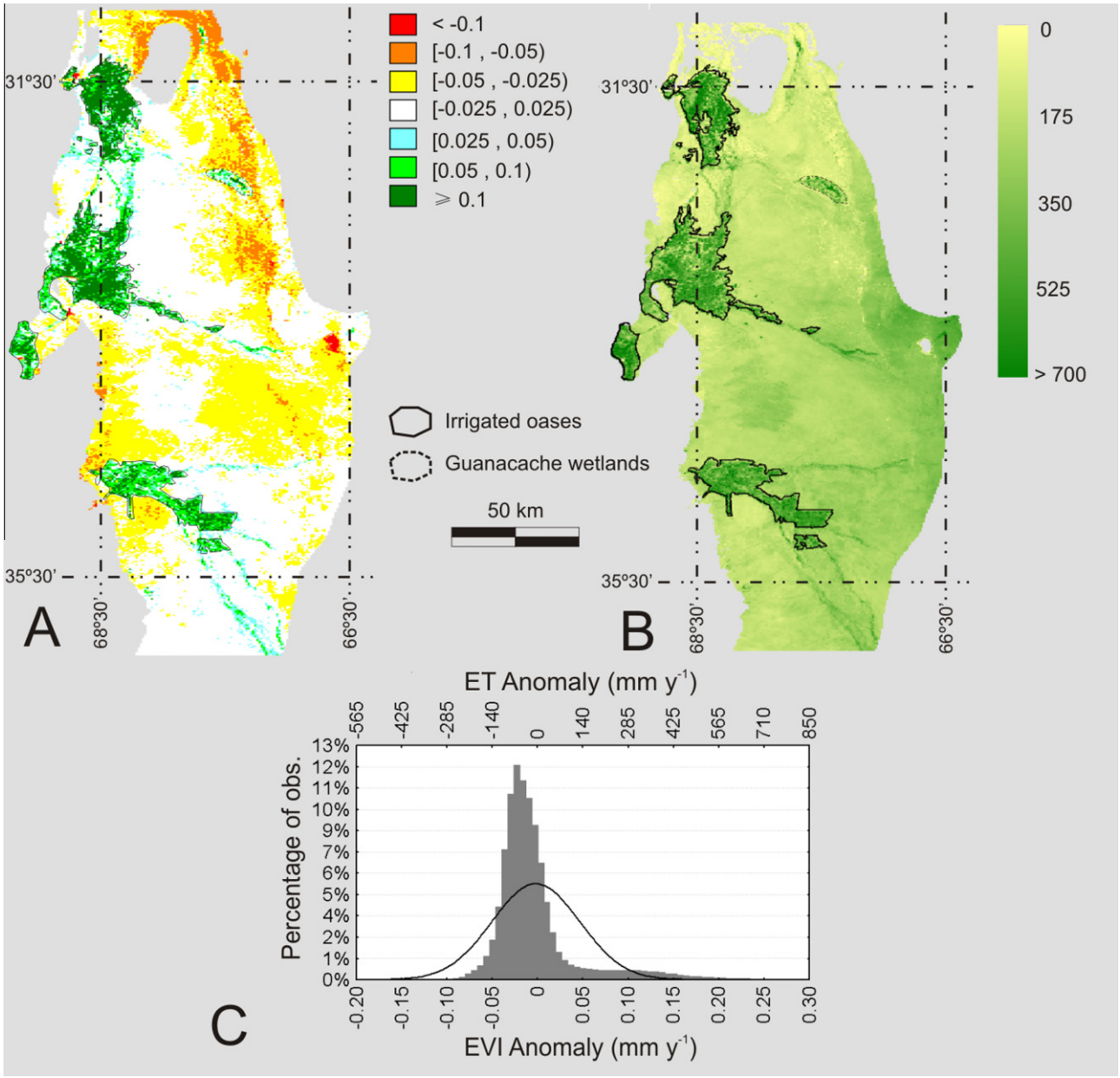


**Fig. 4.** Maps of (A) EVI anomaly classes and (B) mean annual evapotranspiration (mm $y^{-1}$) estimated for the Monte desert region. The histogram of EVI and ET anomalies observed in the study region is shown in graph (C). Solid line in (C) represents the histogram expected for a normal distribution.

mean (±SE) ET values computed from both approaches for olive ($ET_{sat}$ = 889 (±16) vs. $ET_{FAO56}$ = 859 (±7); $n$ = 10; RMSE = 37 mm $y^{-1}$), wine grape ($ET_{sat}$ = 619 (±28) vs. $ET_{FAO56}$ = 649 (±39); $n$ = 10; RMSE = 49 mm $y^{-1}$) and grasslands/pastures stands ($ET_{sat}$ = 685 (±9) vs. $ET_{FAO56}$ = 723 (±8); $n$ = 10; RMSE = 40 mm $y^{-1}$) (Fig. 6). The departures reported between seasonal ET estimates from both approaches suggest that other variables besides the EVI dynamics, e.g. albedo and land surface temperature, would contribute to control the intrannual response of the surface energy/water balance (Kalma et al., 2008 and references therein). How these variables are included in the top-down satellite-based approach proposed here is a topic under study.

Evapotranspiration estimates retrieved from the satellite-based approach for the irrigated areas of San Juan, and Northern, Central, and Southern Mendoza suggested ET anomalies of 626, 402, 246 and 275 mm $y^{-1}$, respectively. These values agreed well with independent estimates based on the water mass balance approach. Differences between both methods ranged from −14% (−31 mm $y^{-1}$) to +20% (+66 mm $y^{-1}$) for the central and southern Mendoza oases respectively (Table 3). In all the oases of the Mendoza province, spatially-aggregated ET anomalies estimated using the mass balance method were within the first and third quartile-boundaries computed from the satellite-based approach. The interannual variability of ET estimated for all the irrigated oases is shown in Fig. 5.

EVI anomalies in artificial oases stress the key role that water extracted from Andean rivers and their associated aquifers play in explaining the evapotranspiration rates observed in artificial oases. In general, Andean rivers are intensively exploited. With 76% of its natural water discharge diverted for irrigation and urban consumption, the Tunuyán (1061 of 1389 $hm^3$ $y^{-1}$) is the most exploited river in the region, followed by the Mendoza (73%; 1041 of 1420 $hm^3$ $y^{-1}$), the Diamante–Atuel (65%; 1528 of 2358 $hm^3$ $y^{-1}$) and the San Juan (53%; ~1100 of 2059 $hm^3$ $y^{-1}$) rivers. Aquifers supplying groundwater represent 17% (339 $hm^3$ $y^{-1}$),

**Table 2**
Remote sensing characterization of natural and cultivated land cover units. Observed EVI, EVI anomaly (observed–expected according to precipitation), annual (mm $y^{-1}$) and seasonal (mm $month^{-1}$) evapotranspiration rates, and mean annual evapotranspiration anomalies (mm $y^{-1}$) show mean and standard errors for each land cover unit. Ten samples of 1 $km^2$ were obtained for each land cover unit, except for "irrigated areas" where 40 samples, ten for each, were selected. Seasons 1 and 2 cover the October–April and May–September periods, respectively.

| Land cover units | EVI observed | EVI anomaly | Mean annual ET | ET (season 1) | ET (season 2) | Mean annual ET anomaly |
|---|---|---|---|---|---|---|
| *Natural systems* | | | | | | |
| Wetlands | 0.30 ± 0.02 | 0.16 ± 0.02 | 672 ± 50 | 92.4 ± 5.3 | 30.0 ± 2.0 | 452 ± 44 |
| Groundwater-fed woodlands | 0.13 ± 0.00 | 0.01 ± 0.00 | 185 ± 7 | 22.6 ± 0.6 | 10.3 ± 0.4 | 23 ± 7 |
| Dunes | 0.09 ± 0.00 | −0.05 ± 0.00 | 64 ± 13 | 7.3 ± 0.3 | 4.0 ± 1.7 | −132 ± 10 |
| Salty areas | 0.08 ± 0.00 | −0.09 ± 0.01 | 34 ± 10 | 3.8 ± 0.8 | 2.2 ± 0.2 | −255 ± 16 |
| *Artificial systems* | | | | | | |
| Non-salinized irrigated croplands | 0.27 ± 0.02 | 0.13 ± 0.01 | 586 ± 22.49 | 82.1 ± 2.5 | 25.0 ± 0.9 | 381 ± 29 |
| San Juan | 0.29 ± 0.02 | 0.20 ± 0.02 | 641 ± 54 | 91.2 ± 6.1 | 26.5 ± 1.8 | 563 ± 54 |
| Northern Mendoza | 0.26 ± 0.01 | 0.14 ± 0.01 | 565 ± 33 | 77.3 ± 3.4 | 25.5 ± 1.5 | 412 ± 33 |
| Central Mendoza | 0.27 ± 0.02 | 0.10 ± 0.02 | 582 ± 45 | 83.6 ± 5.0 | 23.4 ± 1.6 | 261 ± 46 |
| Southern Mendoza | 0.26 ± 0.01 | 0.10 ± 0.01 | 555 ± 41 | 76.3 ± 3.9 | 24.8 ± 2.2 | 289 ± 43 |
| Salinized irrigated croplands | 0.19 ± 0.02 | 0.07 ± 0.02 | 340 ± 45 | 45.8 ± 5.0 | 15.9 ± 1.7 | 210 ± 48 |

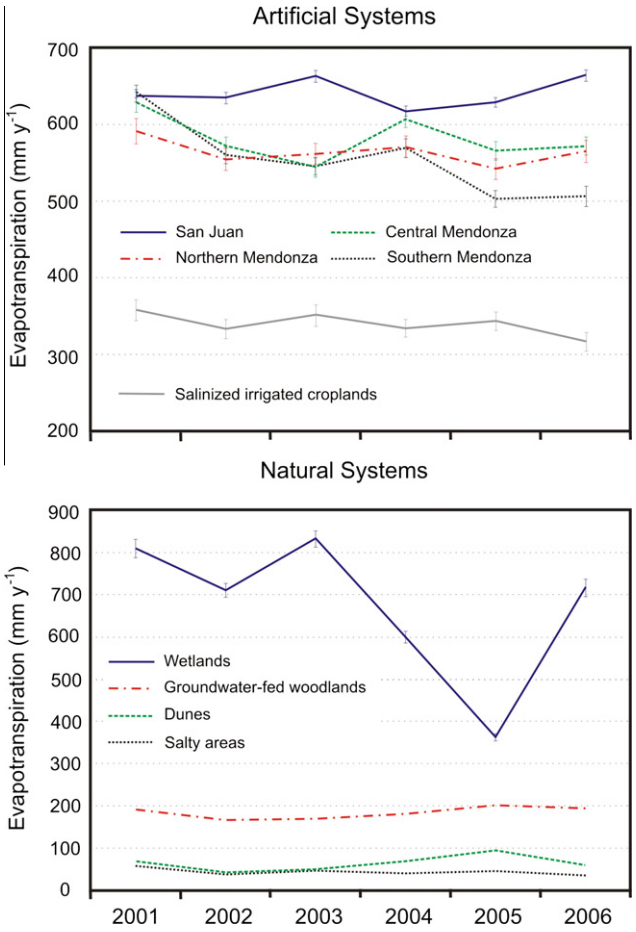


**Fig. 5.** Interannual variability of ET estimated for the irrigated oases located in the region and for several representative natural land cover types in the Monte desert. Standard errors are shown as vertical bars.

50% (195 $hm^3\ y^{-1}$) and 4% (66 $hm^3\ y^{-1}$) of the gross water demands in the northern, central and southern Mendoza oases, respectively (Table 3). However and despite the high water extraction rates from Andean rivers, a large volume of this water ultimately recharges the aquifers because of the low efficiencies of the conveyance/distribution and application systems reported in the oases. Recharge related to irrigation, also termed "human induced recharge", reached values of 1020, 990 and 150 $hm^3\ y^{-1}$ in the northern, southern and central oases, respectively. This recharge, however, is likely taking place at different locations than those, where natural recharge occurred in the past.

## 4. Discussion and conclusions

Our work suggests that satellite-based approaches that rely on ecological principles for estimating the water balance of drylands could have great benefits in areas with poor ground information availability. Based on the long-term precipitation-light absorption (leaf area)-evapotranspiration linear relationship suggested by the hydrological equilibrium hypothesis for water-limited ecosystems (Nemani and Running, 1989), the remote sensing approach and its related biophysical indexes proposed in this research were used to quantify the imprint of remote water resources on the evapotranspiration of desert ecosystems. Both indexes are computed from the spatial analysis of the anomalies defined by an observed spectral vegetation index (EVI) and a potential value which should be previously estimated from a long-term regional rainfall-EVI function. The first index, the EVI anomaly, is related to the ecosystem's capacity to absorb photosyntetically active radiation while the second one, the ET anomaly, is interpreted as the volume of supplementary water consumed by vegetation besides the mean annual precipitation (MAP). Although difficult to obtain regionally, the use of MAP–EVI (or NDVI instead EVI) functions are commonly used in land degradation and desertification monitoring studies (Prince et al., 1998; Boer and Puigdefábregas, 2005; Wessels et al., 2008) in an attempt to derive long-term average reference conditions to which current conditions could be compared and subsequently related to landscape health or functionality properties. Several procedures ranged in a gradient of empiricism have been suggested to extract those functions: from techniques which select non-degraded sites close to protected areas as reference sites (Garbulsky and Paruelo, 2004) to semi-empirical modelling frameworks (Boer and Puigdefábregas, 2003; Del Grosso et al., 2008) to complex physically-based models which take into account optimality principles (Raich et al., 1991). Empirical approaches based on quantile regression analyses are commonly used when not enough undisturbed areas can be isolated. In those cases, the quantile selection must be in accordance with the spatial resolution governing the analysis and the prevailing landscape characteristics being highly advisable to perform a sensitivity analysis to evaluate the impact of the quantile selection on final results.

Independent approaches highlighted the good performance of the satellite-based approach proposed in this study. Error bounds

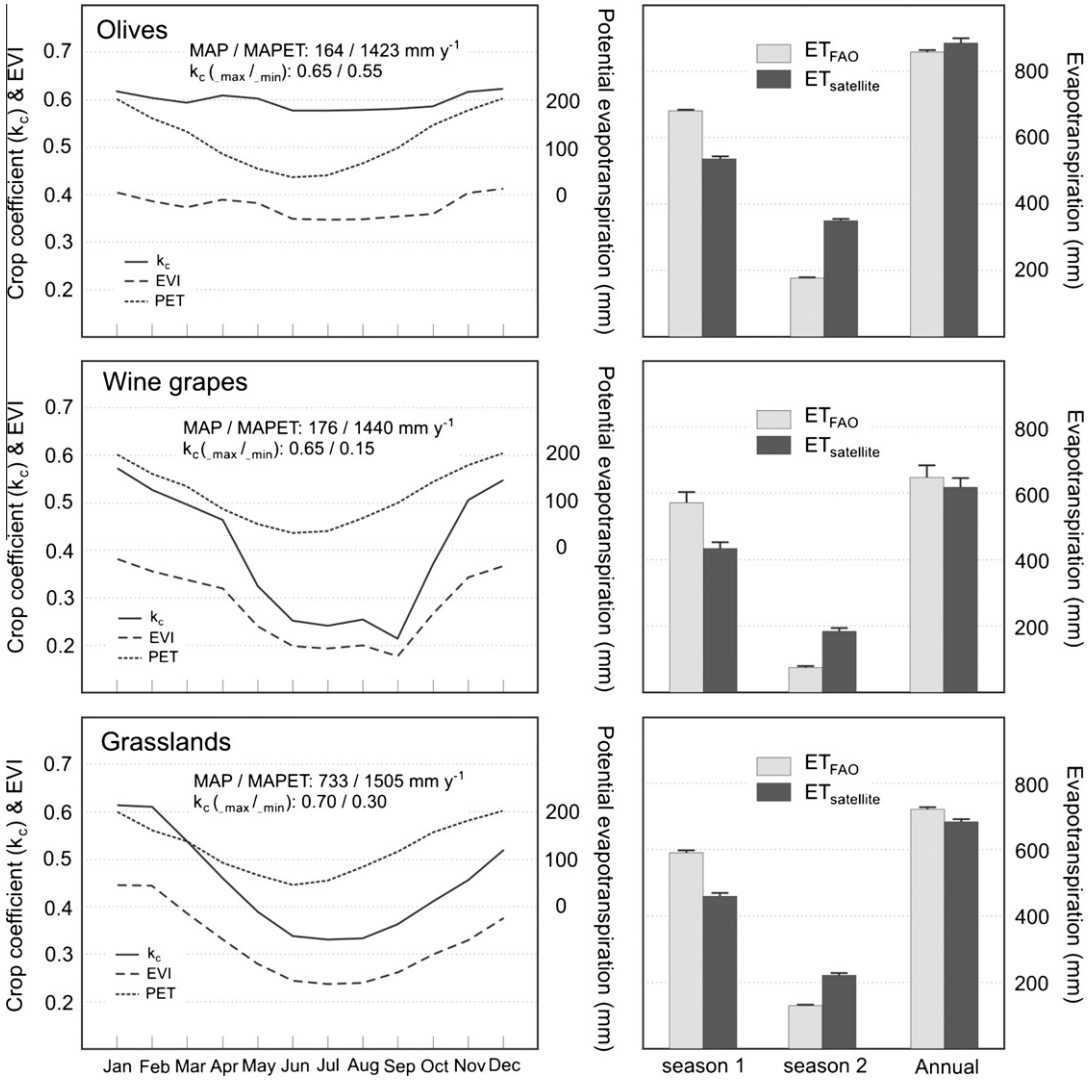


**Fig. 6.** Average monthly variability for EVI, PET and $k_c$ (left panels) and comparison of mean seasonal/annual evapotranspiration rates estimated by the crop coefficient approach ($ET_{FAO}$) and the satellite-based ($ET_{satellite}$) approaches for well-irrigated, non-stressed typical crops (olives and wine grapes) at the Mendoza Central oasis and typical pastures located in the eastern edge of the region (right panels). MAP = mean annual precipitation (mm $y^{-1}$); MAPET: Mean Annual Potential Evapotranspiration (mm $y^{-1}$); $k_c$ = crop coefficient (minimum and maximum values reported by Allen et al., 1998). Standard errors are shown as vertical bars.

found for annual ET in this study (2–15% at plot scale, and 18% at basin scale) were within the range of uncertainty commonly reported for remote sensing approaches (15–30%) by other authors (Glenn et al., 2007; Kalma et al., 2008). The ability of the satellite-based approach to estimate evapotranspiration for different vegetation types and spatial scales suggests that EVI could estimate annual evapotranspiration better than net primary production (NPP). Being a surrogate of the capacity of the canopy to intercept and absorb photsynthetically active radiation, EVI has a closer association with the canopy conductance, controlling both water and carbon fluxes. While the rates of this exchange have a more direct association with ET, their link to NPP involves more complex processes that can create higher departures between NPP and EVI, including plant-dependent physiological differences (e.g. C3 vs. C4 photosynthetic syndrome) or varying rates of respiration decoupling gross C exchange from NPP, and ultimately the efficiency to convert captured light into green biomass (Gamon et al., 1995; Glenn et al., 2008).

Large volumes of water are being actually extracted from Andean rivers to feed artificial oases in the Central Monte desert. According to our results, these rivers and the aquifers that they recharge contribute with 62% (2815 $hm^3$ $y^{-1}$) of the total evapotranspiration (4505 $hm^3$ $y^{-1}$) accounted for all the artificial oases in the region. However, the very low global efficiency of irrigation systems leads to a total detracted volume of 4730 $hm^3$ $y^{-1}$, which represents >60% of the total river discharges and more than five times the total water depth supplied by all the headwater basins of these rivers. These high river extraction rates and the expansion of irrigated land have likely affected the area covered by wetlands in the floodplains. For example, the Rosario–Guanacache wetland, the most important lagoon system in the region, covered a continuous area of 7500–8000 $km^2$ in 1789 but it was completely dried up in 1945 (Abraham and Prieto, 1981). Nowadays, the wetland area approaches 2500 $km^2$ (~2/3 less than the area covered in 1789) and is totally conditioned by intermittent floods. This drastic reduction in the size and flooding frequency of wetlands has been also accompanied by an increase of the area affected by salinization and important reductions of vegetation productivity in the surroundings of the actual wetland boundaries, as observed in the EVI anomalies map (Fig. 4A).

**Table 3**
Main water balance components for the artificial oases of the Mendoza province. All data are given in volume of water ($hm^3\ y^{-1}$) except for efficiencies and EVI anomalies (dimensionless), artificial area (has.), and mean annual precipitation and water depth values estimated for irrigation ($mm\ y^{-1}$). The global irrigation efficiency ($\Gamma_g$) integrates the efficiency of the conveyance and distribution systems ($\Gamma_{cds}$) and the application efficiency estimated at the plot scale ($\Gamma_{fa}$). Water supplies from rivers, *D*, and aquifers, *P*, are referred to annual average values estimated for the period 1991–2000 (Departamento General de Irrigación, 2004b). *U*/*I* values correspond to official statistics for the year 2003. Mean annual precipitation, extracted from the CRU CL 2.0 dataset (New et al., 2002), corresponds to the average value for the period 1961–1990. Cultivated area was computed from the analysis of Landsat imagery taken in 2001 (Departamento General de Irrigación, 2004a). All dispersion statistics are referred to the standard error of the mean.

| Source | Concept | Northern Oasis | Central Oasis | Southern Oasis |
|---|---|---|---|---|
| Fluvial | Volume of water available for consumptive uses, $D$ | 1863 | 238 | 1557 |
| | Diverted for urban and industrial demands, $U/I_F$ | 197 | 1 | 29 |
| | Diverted for irrigation, $D–U/I_F$ | 1666 | 237 | 1528 |
| | Global irrigation efficiency, $\Gamma_g$ ($=\Gamma_{cds} * \Gamma_{fa}$) | 0.39 | 0.38 | 0.14[a] |
| | Actual fluvial supply for irrigation, $ET_F$ (1) | 644 | 90 | 215 |
| Ground-water | Total pumping, $P$ | 397 | 195 | 71 |
| | Pumped for urban and industrial demands, $U/I_{GW}$ | 58 | 0 | 5 |
| | Pumped for irrigation, $P–U/I_{GW}$ | 339 | 195 | 66 |
| | Irrigation efficiency $\Gamma_{fa}$ | 0.56 | 0.56 | 0.40 |
| | Actual groundwater supply for irrigation, $ET_{GW}$ (2) | 190 | 109 | 26 |
| Non-rainfall water supply for irrigation ($hm^3\ y^{-1}$) (1) + (2) | | 834 | 199 | 242 |
| Cultivated area (has.) | | 178,147 | 92,792 | 70,765 |
| Non-rainfall water depth used for irrigation ($mm\ y^{-1}$) | | 468 | 215 | 341 |
| Mean annual precipitation ($mm\ y^{-1}$) | | 161 ± 1 | 316 ± 2 | 264 ± 1 |
| EVI anomaly | | 0.14 ± 0.00 | 0.09 ± 0.00 | 0.10 ± 0.00 |
| Satellite-based Evapotranspiration anomaly ($mm\ y^{-1}$) | | 402 ± 8 | 246 ± 12 | 275 ± 8 |

[a] This figure was computed using a conveyance/distribution efficiency of 0.35 and an application efficiency of 0.4. Both efficiencies contribute to the recharge of the Southern Hydrogeological Unit in 990 $hm^3\ y^{-1}$ and 362 $hm^3\ y^{-1}$, respectively (Departamento General de Irrigación, 2004a).

Because large desert rivers are usually the primary agents of salt transport, dilution, and flushing in these regions, their diversion towards irrigated oases may impact vegetation productivity, water/energy exchange patterns, and whole ecosystem integrity through its effects on salt dynamics (Hillel, 2000; Cai et al., 2003). Secondary salinization caused by inappropriate irrigation practices results from two basic mechanisms. Firstly, insufficient drainage can lead to the accumulation of salts delivered by irrigation waters (i.e., top-down salinization), a process that is promoted by the high evapotranspiration rates and low precipitation inputs of arid regions. Secondly, shifts in the spatial patterns of recharge can lead to rising of water tables that transport salts to the surface, accumulating them through direct soil evaporation (i.e. bottom-up salinization). The salts carried by irrigation waters and those originally stored in the desert territory can feed this process, that becomes more intense in the lowest and/or flatest sections of the artificial oases. Our results indicated an average reduction of 30% of the mean annual EVI in salt-affected croplands, suggesting that "bottom-up" salinization, evidenced by cooler surface temperatures than those expected from EVI values (data not shown), could be the predominant process. In agreement with these observations, groundwater and soil salinity problems have been observed in areas with shallow water tables across all the artificial oases of the region (Foster and Garduño, 2005).

We developed a satellite-based top-down framework based on ecological assumptions to identify inflow dependent ecosystems and quantify the impact of water supplies, in our case from mountains to deserts, on the water balance of drylands. Estimates of evapotranspiration from irrigated areas and natural vegetation in the Andes footslope matched well with existing water budgets and evapotranspiration outputs from complementary techniques, suggesting that this approach can be used for a continuous, spatially explicit, and cost-effective monitoring of evapotranspiration and allocation at the regional scale. The application to the whole Central Monte desert showed that although artificial oases occupy slightly more than one half of the area covered by inflow dependent ecosystems – i.e., wetlands, and riparian and groundwater-fed oases – and ~11% of the study area, they currently consume three to four times more water and 22% of the water that is evapotranspirated in the whole region. The satellite-based method presented here will likely help to assess how artificial oases and inflow dependent ecosystems evolve under the shifting pressures of land use and climate change.

## Acknowledgments

The core of this research was supported by Grant 8277/07 from the National Geographic Society, and Grant CRN 2031 from the Inter American Institute for Global Change Research (after NSF Grant GEO-0452325). First author was granted by a fellowship funded by the IAI and a postdoctoral fellowship awarded by the Spanish Ministry of Science and Technology (2008-0486). We thank Julieta Araníbar for her assistance in collecting the Mendoza Water Management Plans. Bridget Scanlon, Prasanna H. Gowda, Celina Santoni, German Baldi, and three anonymous reviewers are also acknowledged for their insightful comments and technical support.

## Appendix A. Supplementary material

Supplementary data associated with this article can be found, in the online version, at doi:10.1016/j.jhydrol.2010.11.014.

## References

Abraham, E., Prieto, M., 1981. Enfoque diacrónico de los cambios ecológicos y de las adaptaciones humanas en el N.E. Árido mendocino. Cuadernos del Centro de Estudios Interdisciplinarios de Fronteras Argentinas 8, 107–139.

Abraham, E., Rodríguez, F. (Eds.), 2000. Argentina: recursos y problemas ambientales de la zona árida. Tomo I Caracterización Ambiental, Junta de Andalucía/Universidades y Centros de la Región Andina, Buenos Aires, Argentina, 144 pp.

Abraham, E., del Valle, H.F., Roig, F., Torres, L., Ares, J.O., Coronato, F., Godagnone, R., 2009. Overview of the geography of the Monte Desert biome (Argentina). J. Arid Environ. 73, 144–153.

Allen, R.G., Pereira, L.S., Raes, D., Smith, M., 1998. Crop evapotranspiration: Guidelines for computing crop water requirements, FAO Irrigation and Drainage Paper no. 56, Food and Agriculture Organization of the United Nations, Rome, pp. 290.

Austin, A.T., Sala, O.E., 2002. Carbon and nitrogen dynamics across a natural precipitation gradient in Patagonia, Argentina. J. Veg. Sci. 13, 351–360.

Boer, M.M., Puigdefábregas, J., 2003. Predicting potential vegetation index values as a reference for the assessment and monitoring of dryland condition. Int. J. Remote Sens. 24, 1135–1141.

Boer, M.M., Puigdefábregas, J., 2005. Assessment of dryland degradation condition using spatial anomalies of vegetation index values. Int. J. Remote Sens. 26, 4045–4065.

Brown, J.B., Bach, L.B., Aldous, A.R., Wyers, A., DeGagné, J., 2010. Groundwater dependent ecosystems in Oregon: an assessment of their distribution and associated threats. Front. Ecol. Environ.. doi:10.1890/090108.

Cade, B.S., Richards, J.D., 2005. User manual for Blossom Statistical Software, Open File Rep. 2005-1353, US Geol. Surv., Reston, Virginia, pp. 124.

Cai, X., McKinney, D.C., Rosegrant, M.W., 2003. Sustainability analysis for irrigation water management in the Aral Sea region. Agr. Syst. 76, 1043–1066.

Cleugh, H.A., Leuning, R., Mu, Q., Running, S.W., 2007. Regional evaporation estimates from flux tower and MODIS satellite data. Remote Sens. Environ. 106, 285–304.

Contreras, S., Boer, M.M., Alcalá, F.J., Domingo, F., García, M., Pulido-Bosch, A., Puigdefábregas, J., 2008. An ecohydrological modelling approach for assessing long-term recharge rates in semiarid karstic landscapes. J. Hydrol. 351, 42–57.

Cox, R., Barron, A. (Eds.), 1998. Great Artesian Basin, Resource Study, Great Artesian Basin Consultative Council. Forrest, ACT, Australia, p. 235.

Del Grosso, S., Parton, W., Stohlgren, T., Zheng, D., Bachelet, D., Prince, S., Hibbard, K., Olson, R., 2008. Global potential net primary production predicted from vegetation class, precipitation, and temperature. Ecology 89, 2117–2126.

Departamento General de Irrigación, 2004a. Informe de Resultados de Usos de la Tierra Según el Tratamiento Digital de Imágenes de Satélite Landsat Para la Provincia de Mendoza. Report PNUD-FAO-ARG-00/08, Gobierno de Mendoza, Mendoza, Argentina, pp. 27.

Departamento General de Irrigación, 2004b. Planes Directores de los Recursos Hídricos de la Provincia de Mendoza. Report PNUD-FAO-ARG-00/08, Gobierno de Mendoza, Mendoza, Argentina.

Eagleson, P.S., 1982. Ecological optimality in water-limited natural soil–vegetation systems: theory and hypothesis. Water Resour. Res. 18, 235–340.

Eamus, D., 2003. How does ecosystem water balance affect net primary productivity of woody ecosystems? Func. Plant Biol. 30, 187–205.

Ellis, T.W., Hatton, T.J., 2008. Relating leaf area index of natural eucalypt vegetation to climate variables in southern Australia. Agr. Water Manage. 95, 743–747.

Emanuel, R.E., D'Odorico, P., Epstein, H.E., 2007. Evidence of optimal water use by vegetation across a range of North American ecosystems. Geophys. Res. Lett. 34, L07401. doi:10.1029/2006GL028909.

Ezcurra, E. (Ed.), 2006. Global Desert Outlook, UNEP Job No. DEW/0839/NA. United Nations Environment Programme, Nairobi, Kenya, pp. 164.

FAO, 2006. ClimWat 2.0. for CropWat, Food and Agriculture Organization, Rome, Italy. <http://www.fao.org/nr/water/infores_databases_climwat.html>.

Foster, S., Garduño, H., 2005. Argentina: Integrated approaches to groundwater resource conservation in the Mendoza aquifers, GW–MATE Case Profile Collection no. 6, The World Bank, Washington DC, pp. 16.

Gamon, J.A., Field, C.B., Goulden, M.L., Griffin, K.L., Hartley, A.E., Joel, G., Peñuelas, J., Valentini, R., 1995. Relationships between NDVI, canopy structure, and photosynthesis in three Californian vegetation types. Ecol. Appl. 5, 28–41.

Garbulsky, M.F., Paruelo, J.M., 2004. Remote sensing of protected areas to derive baseline vegetation functioning characteristics. J. Veg. Sci. 15, 711–720.

Glantz, M.H. (Ed.), 1999. Creeping Environmental Problems and Sustainable Development in the Aral Sea Basin. Cambridge University Press, Cambridge, UK, p. 304.

Glenn, E.P., Huete, A.R., Nagler, P.L., Hirschboeck, K.K., Brown, P., 2007. Integrating remote sensing and ground methods to estimate evapotranspiration. Crit. Rev. Plant Sci. 26, 139–168.

Glenn, E.P., Huete, A.R., Nagler, P.L., Nelson, S.G., 2008. Relationship between remotely-sensed vegetation indices, canopy attributes and plant physiological processes: what vegetation indices can and cannot tell us about the landscape. Sensors 8, 2136–2160.

González-Loyarte, M.M., Menenti, M., Weidema, P., Roig, F.A., Barton, M., 2000. Mapping vegetation degradation applying remotely sensed data in the arid zones of Argentina. The Northeastern plain of Mendoza. In: Proceedings of United Nations/International Astronautical Federation Workshop on Operational Strategy for Sustainable Development using Space, UN Committee on the Peaceful Uses of Outer Space and Office for Outer Space Affairs, Sao José dos Campos, Brazil.

Godwa, P.H., Chavez, J.L., Colaizzi, P.D., Evett, S.R., Howell, T.A., Tolk, J.A., 2008. ET mapping for agricultural water management: present status and challenges. Irrigation Sci. 3, 223–237.

Greenwood, E.A.N., Klein, L., Beresford, J.S., Watson, G.D., 1985. Differences in annual evaporation between grazed pasture and Eucalyptus species in plantations on a saline farm catchment. J. Hydrol. 78, 261–278.

Groeneveld, D.P., Baugh, W.M., Sanderson, J.S., Cooper, D.J., 2007. Annual groundwater evapotranspiration mapped from single satellite scenes. J. Hydrol. 344, 146–156.

Guerschman, J.P., Van Dijk, A.I.J.M., Mattersdorf, G., Beringer, J., Hutley, L.B., Leuning, R., Pipunic, R.C., Sherman, B.S., 2009. Scaling of potential evapotranspiration with MODIS data reproduces flux observations and catchment water balance observations across Australia. J. Hydrol. 369, 107–119.

Hatton, T.J., Salvucci, G.D., Wu, H.I., 1997. Eagleson's optimality theory of an ecohydrological equilibrium: quo vadis? Funct. Ecol. 11, 665–674.

Hillel, D., 2000. Salinity Management for sustainable irrigation: Integrating science, environment and economics. In: The International Bank for Reconstruction and Development – The World Bank, Washington, DC, USA, report, pp. 92.

Hoff, C., Rambal, S., Joffre, R., 2002. Simulating carbon and water flows and growth in a mediterranean evergreen Quercus ilex coppice using FOREST–BGC model. For. Ecol. Manage. 164, 121–136.

Howard, J., Merrifield, M., 2010. Mapping groundwater dependent ecosystems in California. PLos One 5, e11249.

Huete, A., Didan, K., Miura, T., Rodriguez, E.P., Gao, X., Ferreira, L.G., 2002. Overview of the radiometric and biophysical performance of the MODIS vegetation indices. Remote Sens. Environ. 83, 195–213.

INDEC, 2001. Censo Nacional de Población, Hogares y Viviendas del Año 2001. Instituto Nacional de Estadística y Censos [CD-ROM], Buenos Aires, Argentina.

Jiang, L., Islam, S., Carlson, T.R., 2004. Uncertainties in latent heat flux measurement and estimation: implications for using a simplified approach with remote sensing data. Can. J. Rem. Sens. 30, 769–787.

Jobbágy, E.G., Sala, O.E., Paruelo, J.M., 2002. Patterns and controls of primary production in the Patagonian steppe: a remote sensing approach. Ecology 83, 307–319.

Jobbágy, E.G., Nosetto, M.D., Villagra, P.E., Jackson, R.B., 2010. Water subsidies from mountains to deserts: their role in sustaining groundwater-fed oases in a sandy landscape. Ecol. Appl., doi:10.189/09-1427.1.

Kalma, J.D., McVicar, T.R., McCabe, M.F., 2008. Estimating land surface evaporation: a review of methods using remotely sensed surface temperature data. Surv. Geophys. 29, 421–469.

Knapp, A.K., Smith, M.D., 2001. Variation among biomes in temporal dynamics of aboveground primary production. Nature 291, 481–484.

Kelliher, F.M., Leuning, R., Raupach, M.R., Schulze, E.D., 1995. Maximum conductances for evaporation from global vegetation types. Agr. Forest Meteorol. 73, 1–16.

Kingsford, R. (Ed.), 2006. Ecology of Desert Rivers. Cambridge University Press, Cambridge, UK, p. 368.

Le Houréou, H.N., 1999. Estudios e Investigaciones Ecológicas de las Zonas Áridas y Semiáridas de Argentina. Technical report IADIZA/CRICYT, Mendoza, Argentina, pp. 228.

Lo Seen Chong, D., Mougin, E., Gastellu-Etchegorry, J.P., 1993. Relating the global vegetation index to net primary productivity and actual evapotranspiration over Africa. Int. J. Remote Sens. 14, 1517–1546.

McCabe, M.F., Wood, E.F., 2006. Scale influences on the remote estimation of evapotranspiration using multiple satellite sensors. Remote Sens. Environ. 105, 271–285.

Monteith, J.L., 1988. Does transpiration limit the growth of vegetation or vice versa? J. Hydrol. 100, 57–68.

Mu, Q., Heinsch, F.A., Zhao, M., Running, S.W., 2007. Development of a global evapotranspiration algorithm based on MODIS and global meteorology data. Remote Sens. Environ. 111, 519–536.

Nagler, P.L., Cleverly, J., Glenn, E., Lampkin, D., Huete, A., Wan, Z., 2005. Predicting riparian evapotranspiration from MODIS vegetation indices and meteorological data. Remote Sens. Environ. 94, 17–30.

Nemani, R.R., Running, S.W., 1989. Testing a theoretical climate-soil-leaf area hydrologic equilibrium of forests using satellite data and ecosystem simulation. Agr. Forest Meteorol. 44, 245–260.

New, M., Lister, D., Hulme, M., Makin, I., 2002. A high-resolution data set of surface climate over global land areas. Clim. Res. 21, 1–25.

Noy-Meir, I., 1973. Desert ecosystems: environment and producers. Ann. Rev. Ecol. Syst. 4, 25–32.

Petropoulos, G., Carlson, T.N., Wooster, M.J., Islam, S., 2009. A review of $T_s$/VI remote sensing based methods for the retrieval of land surface energy fluxes and soil surface moisture. Prog. Phys. Geog. 33, 224–250.

Pitman, A.J., 2003. The evolution of, and revolution in, land surface schemes designed for climate models. Int. J. Climatol. 23, 479–510.

Prince, S.D., Brown de Colstoun, E., Kravitz, L., 1998. Evidence from rain use efficiencies does not support extensive Sahelian desertification. Global Change Biol. 4, 359–374.

Raich, J.W., Rastetter, E.B., Melillo, J.M., Kicklighter, D.W., Steudler, P.A., Peterson, P.J., Grace, A.L., Moore III, B., Vörösmarty, C.J., 1991. Potential net primary productivity in South America: application of a global model. Ecol. Appl. 1, 399–429.

Rodríguez-Iturbe, I., Porporato, A., 2004. Ecohydrology of water-controlled ecosystems: soil moisture and plant dynamics. Cambridge University Press, Cambridge.

Schulze, E.D., Kelliher, F.M., Korner, C., Lloyd, J., Leuning, R., 1994. Relationships among maximum stomatal conductance, ecosystem surface conductance, carbon assimilation rate, and plant nitrogen nutrition: a global ecology scaling exercise. Annu Rev Ecol Syst 25, 629–660.

Siebert, S., Döll, P., Feick, S., Hoogeveen, J., Frenken, K., 2007. Global map of irrigation areas, version 4.0.1. Univ. of Frankfurt/Food and Agriculture Organization of the United Nations, Rome, Italy.

Specht, R.L., 1972. Water use by perennial evergreen plant communities in Australia and Papua New Guinea. Aust. J. Bot. 20, 273–299.

Subsecretaría de Recursos Hídricos, 2004. Estadística hidrológica de la República Argentina [CD-ROM], EVARSA, Buenos Aires, Argentina.

Sun, Z., Wang, Q., Matsushita, B., Fukushima, T., Ouyang, Z., Watanabe, M., 2009. Development of a Simple Remote Sensing EvapoTranspiration model (Sim-ReSET): algorithm and model test. J. Hydrol. 376, 476–485.

Tao, H., Gemmer, M., Song, Y., Jiang, T., 2009. Ecohydrological responses on water diversion in the lower reaches of the Tarim River. China. Water Resour. Res. 44, W08422. doi:10.1029/2007WR006186.

Van Dijk, A.I.J.M., 2010. The Australian Water Resources Assessment System. Technical Report 3. Landscape Model (version 0.5) Technical Description. CSIRO: Water for a Healthy Country National Research Flagship.

Venturini, V., Islam, S., Rodriguez, L., 2008. Estimation of evaporative fraction and evapotranspiration from MODIS products using a complementary based model. Remote Sens. Environ. 112, 132–141.

Villagra, P.E., Defossé, G.E., del Valle, H.F., Tabeni, S., Rostagno, M., Cesca, E., Abraham, E., 2009. Land use and disturbance effects on the dynamics of natural ecosystems of the Monte Desert: implication for their management. J. Arid Environ. 73, 202–211.

Wessels, K.J., Prince, S.D., Reshef, I., 2008. Mapping land degradation by comparison of vegetation production to spatially derived estimates of potential production. J. Arid Environ. 72, 1940–1949.

Zhang, K., Kimball, J.S., Mu, Q., Jones, L.A., Goetz, S.J., Running, S.W., 2009. Satellite based analysis of northern ET trends and associated changes in the regional water balance from 1983 to 2005. J. Hydrol. 379, 92–110.

Zhang, Y.Q., Chiew, F.H.S., Zhang, L., Leuning, R., Cleugh, H.A., 2008. Estimating catchment evaporation and runoff using MODIS leaf area index and the Penman–Monteith equation. Water Resour. Res. 44, W10420. doi:10.1029/2007WR006563.